Carbohydrate Polymers 164 (2017) 379–385

Contents lists available at ScienceDirect

Carbohydrate Polymers

journal homepage: www.elsevier.com/locate/carbpol

Toward novel antiparasitic formulations: Complexes of Albendazole desmotropes and β-cyclodextrin

Ana K. Chattah[a], Laura Y. Pfund[b], Ariana Zoppi[c], Marcela R. Longhi[c], Claudia Garnero[c,*]

[a] Facultad de Matemática, Astronomía y Física and IFEG (CONICET), Univme_checkersidad Nacional de Córdoba, Ciudad Universitaria, X5000HUA Córdoba, Argentina
[b] Department of Chemistry and the Macromolecular Science and Engineering Program, The University of Michigan, Ann Arbor, MI 48109-1055, United States
[c] Departamento de Farmacia, Facultad de Ciencias Químicas and UNITEFA (CONICET), Universidad Nacional de Córdoba, Ciudad Universitaria, X5000HUA Córdoba, Argentina

ARTICLE INFO

Article history:
Received 29 December 2016
Received in revised form 26 January 2017
Accepted 28 January 2017
Available online 3 February 2017

Keywords:
Albendazol
Desmotrope
Cyclodextrin
Characterization
Solubility
Dissolution

ABSTRACT

Novel complexes of two different solid forms of Albendazol and β-cyclodextrin were investigated in an attempt to obtain promising candidates for the preparation of alternative matrices used in pharmaceutical oral formulations. The interaction between each form of Albendazol and β-cyclodextrin was studied in solution and solid state, in order to investigate their effect on the solubility and dissolution rate of Albendazol solid forms. The solid supramolecular systems were characterized using a variety of techniques including natural-abundance ^{13}C cross-polarization magic-angle-spinning nuclear magnetic resonance, powder X-ray diffraction, Fourier transform-infrared spectroscopy and scanning electron microscopy. The results obtained showed the highest increment of solubility and dissolution rate, in simulated gastric fluid, for the Albendazole II:β-cyclodextrin systems. Thus, these new complexes constitute an interesting alternative for improving the oral bioavailability of Albendazol.

1. Introduction

A better understanding of the solid-state interactions in multicomponent pharmaceutical solids can allow for the rational design of novel materials. The solid state characterization of these solids is recognized as an essential part of preformulation research. Additionally, the pharmaceutical solids can exist in different crystalline solid forms. This behavior is known as polymorphism, and affects the chemical and physical properties of active pharmaceutical ingredients (API) including solubility, bioavailability, and stability (Bauer, 2008; Hilfiker, 2006), which have a significant impact on the pharmaceutical industry.

Albendazole (ABZ, Scheme 1), a benzimidazole carbamate, is one of the most effective broad-spectrum anthelmintic agents with activity against human and animal parasites (Barrera et al., 2010; Cook, 1990; García et al., 2013). After oral administration, the API must dissolve in gastric fluid in order to be absorbed; therefore, ABZ therapeutic response is unpredictable due to its low and erratic oral bioavailability caused by poor water solubility and slow dissolution rate. Thus, ABZ has to be administrated in multiple doses in order to provide therapeutic concentrations for an acceptable anthelmintic efficacy (Cook, 1990). However, with high permeability through the biological membranes, ABZ belongs to biopharmaceutical classification system type II (BCS class II) (Lobenberg & Amidon, 2000). Besides, two solid forms have been reported for this API designated as ABZI and ABZII (Chattah et al., 2015; Pranzo, Cruickshank, Coruzzi, Caira, & Bettini, 2010), which are related enantiotropically. The desmotropy of ABZ has been previously described by our group, revealing different tautomeric states for ABZ I and II in solid state (Chattah et al., 2015).

Additionally, the very low water solubility of ABZ impairs its formulation considerably, limiting its administration routes. Therefore, different approaches have been previously investigated to improve the physicochemical properties of ABZ with the goal of optimizing the chemotherapeutic treatment. In previous reports, liposomes (Dvoroznáková, Hrcková, Borosková, Velebny, & Dubinsky, 2004), solid dispersions (Pensel et al., 2014) and cyclodextrins (Codina et al., 2015; Evrard et al., 2002; Ferreira et al., 2015; Pradines et al., 2014) have been used to increase the solubility, the dissolution rate and/or the bioavailability of ABZ. However, these studies have not considered the different solid forms of this API. Having in mind the improvement on the solubility and dissolution behavior of ABZ and the selection of a proper desmotrope for its pharmaceutical use, the aim of the present work is to

* Corresponding author.
E-mail address: garneroc@fcq.unc.edu.ar (C. Garnero).

http://dx.doi.org/10.1016/j.carbpol.2017.01.098
0144-8617/

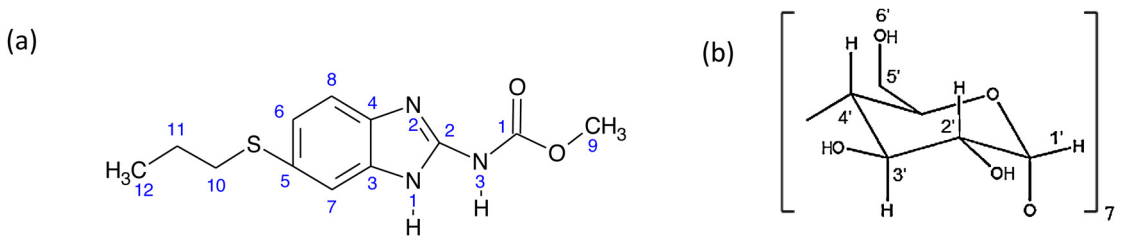

Scheme 1. (a) ABZ and (b) βCD with the carbon numbering used in NMR spectra.

synthesize and characterize novel complexes of the two solid forms of ABZ with β-cyclodextrin (βCD, Scheme 1).

2. Experimental

2.1. Chemicals and reagents

Albendazole (ABZ) was provided by Todo Droga (Argentina), βCD (MW = 1135) was kindly supplied by Ferromet agent of Roquette (France), while BrK was purchased from Merck (Germany). Methanol, analytical reagent grade, was purchased from Cicarelli (Argentina). A Millipore Milli Q Water Purification System (Millipore, Bedford, MA, USA) generated the water used in these studies. All other chemicals were of analytical grade.

2.2. Obtaining the form II of Albendazole

The solid form II of ABZ was recrystallized from a methanol solution as it was previously reported (Pranzo et al., 2010). ABZ form I that corresponds to the commercially available ABZ was dissolved in methanol, heated and stirred until a clear solution was formed. Then, the solution was filtered, followed by slow evaporation of the solvent under ambient conditions, until crystallization was complete. Light brown crystals were collected after 10 days.

2.3. Solubility studies

The effects of βCD on the solubility of solid forms of ABZ were studied in aqueous and simulated gastric fluid without enzymes. The solubility measurements were performed according to the method of Higuchi and Connors (Higuchi & Connors, 1965). An excess of ABZ (forms I and II, respectively) was added to solutions containing increasing concentrations of βCD, which range from 2.5 to 14 mM. ABZ forms I and II, in the absence of βCD, were used to determine the intrinsic solubility. The suspensions were agitated for a speed range from 100 to 200 rpm, maintained at 37.0 ± 0.1 °C for 72 h in an orbital incubator shaker (Agitador Ferca, Argentina). Then, the remaining solid ABZ was removed by filtration through a 0.45 μm membrane filter (Millipore, USA). The clear solutions were suitably diluted and analyzed by UV–Vis spectrophotometry (Agilent Carry 60 spectrophotometer) at λ = 291 nm.

2.4. Preparation of solids samples

Solid-state systems of ABZI and ABZII in equimolar ratio with βCD were prepared as follows.

2.4.1. Kneading method (KN)

The systems ABZI:βCD (KN I) and ABZII:βCD (KN II) were prepared by weighing appropriate amounts of βCD accurately and then transferring them to a mortar. A methanol–water (50:50, v/v) mixture was added to the βCD powder and the resultant slurry was kneaded for about 10 min. For each system, the corresponding solid form of ABZ was added in small portions with the simultaneous addition of solvent in order to maintain a suitable consistency. This slurry was kneaded thoroughly for about 45 min, and the resultant paste was dried in vacuum at 45 °C for 48 h, and protected from light.

2.4.2. Co-precipitation method (CP)

Co-precipitate systems ABZI:βCD (CP I) and ABZII:βCD (CP II) were prepared as follows. The aqueous solution of βCD was added to a methanolic solution of ABZ. The resulting mixture was stirred for 1 h and then the suspensions were allowed to stand for 72 h at room temperature to achieve precipitation. The resultant co-precipitates were removed by filtration and the solids were dried in vacuum at 45 °C for 48 h, and protected from light.

2.4.3. Physical mixture (PM)

Physical binary mixtures of ABZI:βCD (PM I) and ABZII:βCD (PM II) were prepared by simply blending the corresponding components uniformly with a mortar and pestle.

2.5. Solid-state NMR (ssNMR) spectroscopy

High-resolution solid-state ^{13}C spectra of the kneading complexes (KN I, KN II), the co-precipitated samples (CP I and CP II) and the physical mixtures (PM I, PM II) were recorded using the ramp cross polarization/magic angle spinning (CP-MAS) sequence with proton decoupling during acquisition (Harris, 1994). All ssNMR experiments were performed at room temperature in a Bruker Avance II spectrometer equipped with a 4 mm MAS probe, operating at 300.13 MHz for protons. The operating frequency for carbons was 75.46 MHz. Glycine was used as external reference for the ^{13}C spectra and to set up the Hartmann–Hahn matching condition in the cross-polarization experiments. All the spectra were recorded with 1600 scans, a contact time of 1.5 ms during CP and a recycling time of 5 s. The spinning rate for all the samples was 10 kHz. ^{1}H spin-lattice relaxation times in the laboratory frame (^{1}H T_1) were measured for the samples under static conditions with an *inversion-recovery* pulse sequence (π–t–$\pi/2$) with recovery times t between 10 μs and 32 s. The recycling delay in these experiments was 10 s.

2.6. Powder X-ray diffraction (PXRD)

Powder X-ray diffraction patterns were obtained at ambient temperature using a Bruker D8 Advance diffractometer, operating at 40 kV and 40 mA with Cu-Kα radiation (1.5406 Å). All samples were packed into the depression of an indented quartz slide. The powder pattern was collected by scanning 2θ from 3° to 70° with a step size of 0.04° at a scanning rate of 1.5 s/step.

2.7. FT-IR spectroscopy

The FT-IR spectra were recorded on a Nicolet 5 SXC FT-IR Spectrophotometer (Madison, WI, USA). The potassium bromide disks were prepared by compressing the powder.

2.8. Scanning electron microscopy studies (SEM)

Microscopic morphological structures of the raw materials and the solid-state systems were investigated and photographed using a Carl Zeiss Σigma scanning electron microscope. The samples were fixed on a brass stub using a double-sided aluminum tape, which were gold-coated under vacuum by employing a sputter coater Quorum 150 to improve the conductivity.

2.9. Dissolution study

The dissolution profiles of ABZ (forms I and II) and the systems KN I, KN II, CP I, CP II, PM I and PM II were evaluated in a dissolution apparatus (Hanson SR II 6 Flask Dissolution Test Station, Hanson Research Corporation, Chatsworth, CA, USA), using the paddle method according to USP apparatus 2, at a temperature of 37.0 ± 0.5 °C and rotation speed of 50 rpm. Suitable quantities of each powder containing about 50 mg of API were compressed using a hydraulic press at an appropriate force to obtain discs, which will not be disintegrated under the test conditions. The discs were immersed into 500 ml of the dissolution medium that simulated gastric fluid without enzymes. Aliquots of the dissolution sample were collected at appropriate time intervals, with immediate replacement by equal volumes of fresh medium maintained at the same temperature. Each sample was filtered, adequately diluted with dissolution media and analyzed for API content by spectrophotometry (Agilent Carry 60 spectrophotometer) at 291 nm. Cumulative percentages of the API released from the discs were calculated. All the experiments were performed in triplicate. The results were expressed as mean % of API released (±SD) at the given sampling time.

The comparison of dissolution profiles was performed using the similarity factor (f_2) (Moore & Flanner, 1996), which is a model adopted by several guidances as a criterion for estimating the closeness between in vitro dissolution profiles (Costa, 2001) as:

$$f2 = 50\log\{\left[1 + \frac{1}{n}\sum_{t=1}^{n}(R_t - T_t)^2\right]^{-0,5} 100\} \quad (1)$$

where n is the number of sampling points, and R_t and T_t are the percentages dissolved of the reference and the test product, respectively, at each time point t. For curves to be considered similar, the $f2$ values should be close to 100. Generally, $f2$ values are greater than 50 (50–100), which implies an average difference of no more than 10% at the sample time points. This ensures equivalence of the two curves and, thus, of the performance of the test and the reference products.

3. Results and discussion

3.1. Phase solubility analysis

Solubility improvement can enhance oral bioavailability of BCS class II as ABZ. A strategy especially effective is the complex formation with CD. ABZ is weakly basic in nature (has two pK_a values of 2.68 and 11.83); therefore, its solubility is higher at lower pH rather than at neutral and basic pH. Hence, in order to determine the influence of the pH and the effect of βCD on the solubility of both solid forms, ABZI and ABZII, phase solubility diagrams were obtained in aqueous and simulated gastric fluid solutions at 37.0 ± 0.1 °C. Fig. 1 shows the diagrams obtained by plotting the changes in ABZ solubility as a function of βCD concentration.

The interactions of the ABZI:βCD and ABZII:βCD systems in aqueous solutions displayed typical A_N type solubility diagrams (Fig. 1a). The negative deviation from linearity at higher

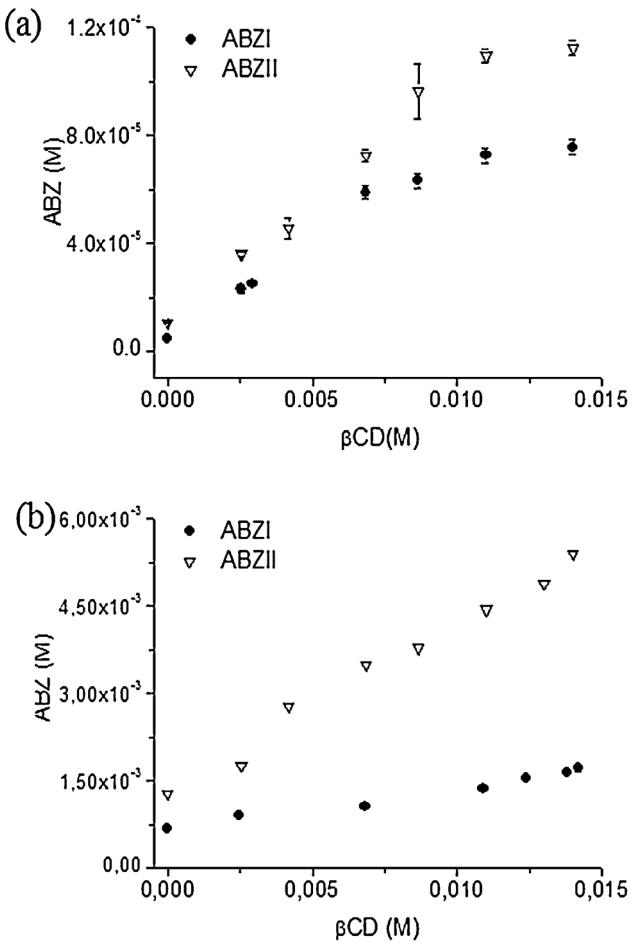

Fig. 1. Effect of βCD on the solubility of ABZI and ABZII in (a) aqueous and (b) simulated gastric fluid solutions.

concentrations of these curves may be originated from both an alteration in the effective nature of the solvent, in the presence of large concentrations of βCD, and a self-association of βCD at higher concentrations (Brewster & Loftsson, 2007; Higuchi & Connors, 1965). The initial ascending portion of the diagram had a slope lower than 1, which indicated that a soluble inclusion complex with a 1:1 molar ratio was formed at low βCD concentrations. The solubility curves obtained for both systems in simulated gastric fluid were of A_L type (Fig. 1b) (Brewster & Loftsson, 2007; Higuchi & Connors, 1965), indicating the formation of soluble binary complexes of a presumable 1:1 stoichiometry.

These studies revealed that ABZ solubility is strongly dependent on the properties of solid state. Different solubility behaviors were determined, being ABZII more soluble than ABZI. Whereas form I had the highest intrinsic solubility in water, ABZII had a greater solubility in simulated gastric fluid.

The apparent stability constant (K_C) values, shown in Table 1, were estimated from the slope of the initial linear portion of the diagrams and the intrinsic solubility of each polymorph (S_0), according to the following equation:

$$K_C = \text{slope}/S_0\,(1 - \text{slope}) \quad (2)$$

According to the K_C values, it can be observed that the ionization affected the interaction of the each ABZ solid form with βCD. In particular, we observed that βCD in aqueous solution significantly increased the apparent solubility of each ABZ solid form. These results showed that drug–cyclodextrin complexation has been better with ionized ABZ in aqueous solution, while the achieved total

Table 1
Summary of solubility studies at 37.0 ± 0.1 °C.

Solvent	ABZ I:βCD				ABZ II:βCD			
	S_0 (μg/ml)	S_{max} (μg/ml)	Solubility increased (S_{max}/S_0)	K_C (M^{-1})	S_0 (μg/ml)	S_{max} (μg/ml)	Solubility increased (S_{max}/S_0)	K_C (M^{-1})
Water	1.2	19.9	16.6	1567	2.8	29.8	10.6	889
Simulated gastric fluid	183	472	2.6	371	320	1467	4.6	345

solubility was higher when the ABZ was unionized in simulated gastric fluid. Although the greatest increase in solubility occurred in aqueous solution, the amount dissolved is still very small. Besides, it can be noted that the highest solubility value was shown by the ABZII:βCD system in simulated gastric fluid. Additionally, the K_C values clearly demonstrate, within experimental error, that both ABZ forms had similar affinity for βCD in simulated gastric fluid.

3.2. Solid state characterization

3.2.1. ssNMR

Solid state NMR (ssNMR) is an unvaluable tool to prove intermolecular interactions that lead to complex formations and solid phase transformations (Monti, Chattah, & Garro Link, 2014). Fig. 2(a, b) displays the ^{13}C CP-MAS spectra of ABZI and ABZII in comparison with the corresponding PM and the KN and CP systems with βCD. The carbon numbering of the ABZ and βCD molecules is displayed in Fig. 1. The ^{13}C CP-MAS spectrum of βCD, extensively reported in the literature (not shown), displays multiple and sharp resonances for each type of carbon (in the region 50–110 ppm), typical of crystalline systems corresponding to distinct values of dihedral angles of the glycosidic alfa(1 → 4) bond for carbons 1 and 4, and with torsion angles describing the orientation of the hydroxyl groups (Braga, Goncalves, Herdtweck, & Teixeira Dias, 2003; Gao et al., 2006; Zoppi et al., 2011). In the figure, different factors of amplifications have been applied for the systems in order to distinguish the ABZ signals. The carbon signal assignments of both solid forms ABZI and ABZII can be observed in our previous report (Chattah et al., 2015), were each solid form was well distinguished. It is interesting to note that, as it occurs in most of our analyzed cases (Chattah et al., 2013; Garnero, Chattah, & Longhi, 2013; Garnero, Chattah, & Longhi, 2014), carbon signals of βCD are well separated in the carbon domain from the signals corresponding to the active principle.

PM I and PM II display a combination of the separate ABZ and βCD spectra, without great evidence of interactions in the mixtures, although some signals corresponding to the βCD become wider. Indeed, PM I and PM II spectra look different in the region corresponding to the ABZ (I or II). It is also possible to see that KN (I and II) spectra and their corresponding PM display differences, mainly in the region of βCD, where (C1'–C6') broadened and some of them merged, forming groups of wide signals in the 50–110 ppm range. This fact indicates that a solid-phase transformation has occurred, and the complexes are new solid forms. There are some changes in the region regarding ABZ signals, corresponding to carbon 16 in KN I and carbon 14 in KN II, which display an extra signal. Comparing KN I and KN II, they display quite different spectra, as it was expected. Regarding CP I, the spectra look quite different to the PM I with some shifts, changes in intensities and the appearance of new signals at 93, 96 and 48 ppm giving evidence that the precipitate is a new solid form. In CP II, the changes are minor in comparison to PM II, mostly in the region of the βCD, and, again, there is an extra signal at 48 ppm, which is indicative of the complex formation. Moreover, the presence of ABZ signals with similar chemical shifts, as in the free drug spectrum in all the systems KN and CP, suggests that a certain amount of pure drug remained, without interaction with βCD, as it has been previously observed in other complexes with βCD. On the other side, CP I and II can be distinguished from their ^{13}C spectra both in the βCD and ABZ regions.

Additional information on the complex formation was obtained by ^1H T_1 relaxation time experiments performed in the pure compounds, PM and complexes. To determine the ^1H T_1 values from the inversion recovery experiments, the broad ^1H spectrum was integrated. Then the behavior of ^1H magnetization as a function of the recovery time was fitted using one or two relaxation times.

The pure ABZ solid forms led to single and distinguished values of T_1 (2.02 s for I and 3.81 s for II) with an order of magnitude different to that of βCD (1.0 s). The PMs led to two relaxation times, one close to the βCD value with major proportion and the other similar to the ABZ component with less proportion. In the complexes, a distinct value corresponding to the sample with the major proportion (80%) can be seen, and it is around 1.5 s in CP I, 1.3 s in CP II, and around 1.7 s in the KN systems. These confirmed the fact that the KNs and CPs are new solid forms originated from the interactions between ABZ and the βCD, and that can be distinguished from their precursors.

3.2.2. PXRD

In order to characterize the powders, we performed PXRD experiments; the diffractograms are shown in Fig. 3.

The PXRD patterns for each ABZ solid forms and βCD showed good agreement with those in the literature (Chattah et al., 2015; Delrivo, Zoppi, & Longhi, 2012). However, the PXRD patterns for KN and CP systems displayed significant different reflections with

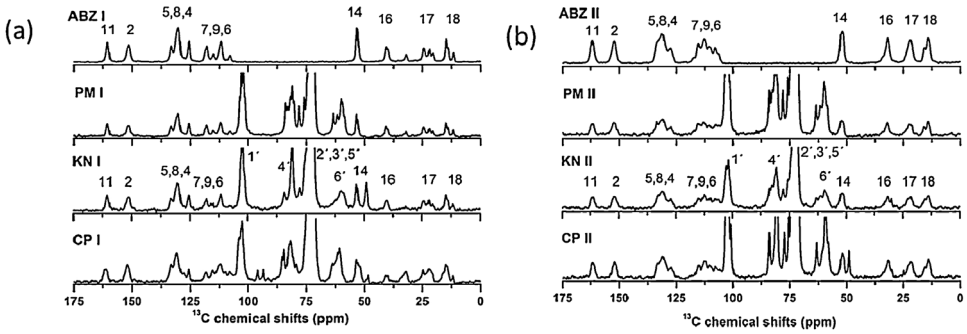

Fig. 2. ^{13}C CP-MAS spectra of: (a) ABZ I:βCD systems and (b) ABZ II:βCD systems obtained by kneading (KN) and co-precipitation (CP) methods and physical mixture (PM).

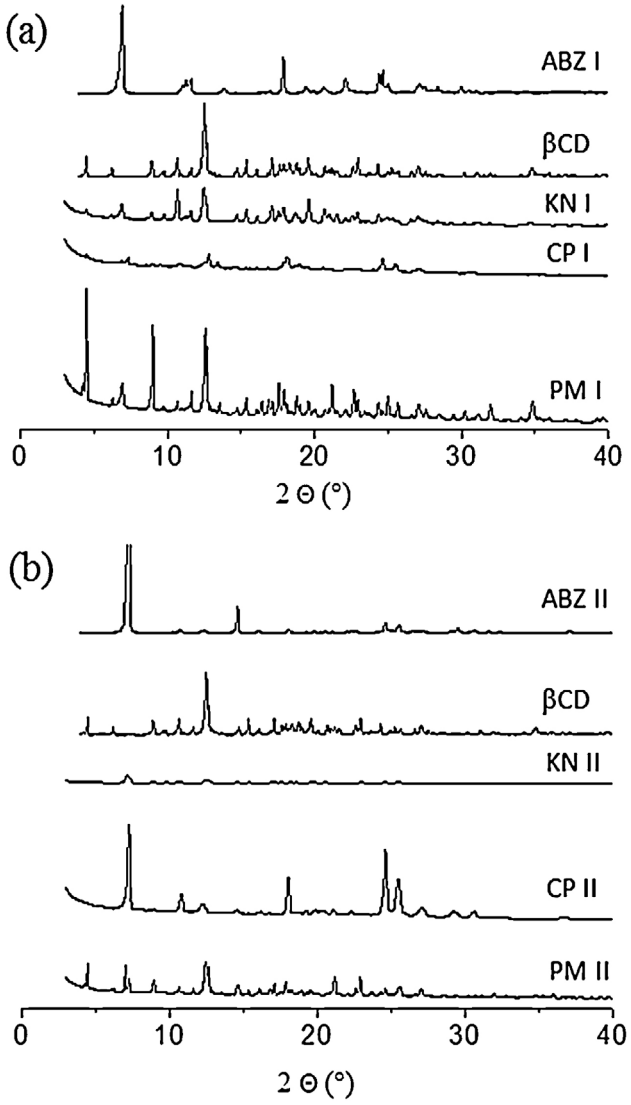

Fig. 3. Powder X-ray diffraction patterns of: (a) ABZ I:βCD systems and (b) ABZ II:βCD systems obtained by kneading (KN) and co-precipitation (CP) methods and physical mixture (PM).

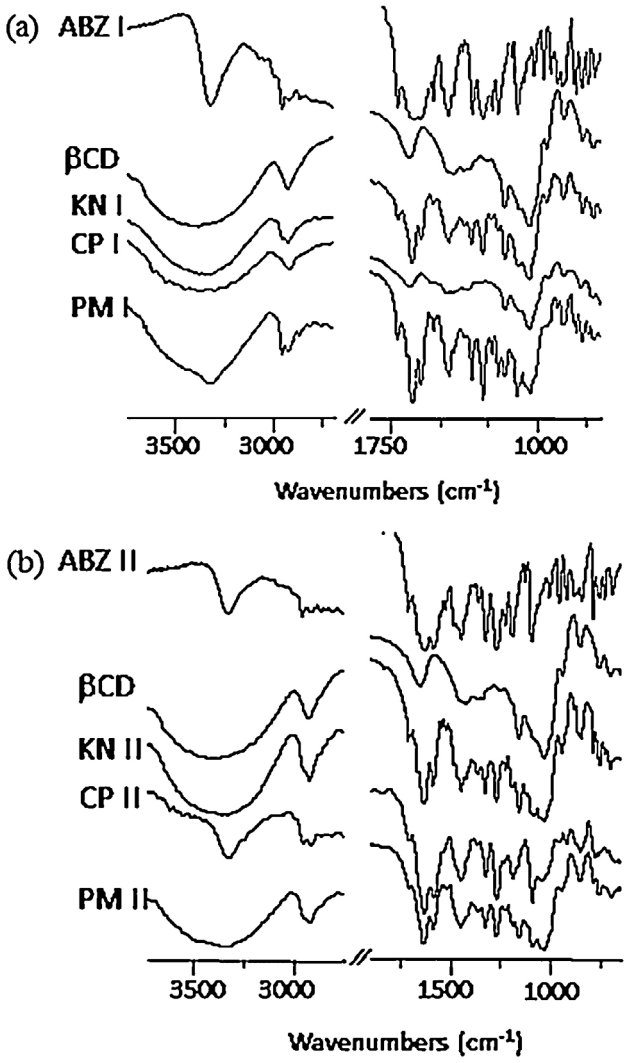

Fig. 4. FT-IR spectra of: (a) ABZ I:βCD systems and (b) ABZ II:βCD systems obtained by kneading (KN) and co-precipitation (CP) methods and physical mixture (PM).

respect to the components alone. Particularly, characteristic new peaks were observed at 14.7° in KN I; at 7.3°, 10.9°, 13.5° and 18.2°, in CP I; at 7.2°, 10.6° and 12.6° in KN II; and at 12.3° and 19.9° in CP II. Furthermore, by examining the PXRD patterns for KN I, KN II, CP I and CP II, it is apparent that all of these were different materials. Additionally, it was possible to differentiate the PXRD patterns of the PMs, KNs and CPs. These results are a good indication that allowed us to suggest that new solid forms were obtained by KN and CP.

3.2.3. FT-IR

Segments of the FT-IR spectra of ABZ, βCD, their corresponding CPs, KNs and PMs systems are shown in Fig. 4. Both ABZ solid forms were characterized previously (Chattah et al., 2015). Their FT-IR spectra reveal marked differences that allow distinguishing between both solid forms.

In the FT-IR spectrum of KN I, the band at 2953 cm^{-1} (assigned to the bond C–H in CH_3 vibrations) disappeared, while the bands at 1708 cm^{-1} (carbonyl group), 1636 and 1454 cm^{-1} were widened, and the bands at 1325 cm^{-1} (C–N amide) and 1092 cm^{-1} (C–O–C ether) were shifted at 1329 and 1089 cm^{-1}, respectively. In the case of CP I, the bands at 2953 and 1708 cm^{-1} disappeared, and the bands at 2926 and 657 cm^{-1} were shifted to lower frequencies of 2915 and 652 cm^{-1}, respectively. On the other hand, the spectrum for KN II showed the band at 2957 cm^{-1} unchanged, while the band at 2912 cm^{-1} was shifted to a higher frequency of 2922 cm^{-1}, the characteristic band of carbonyl group was shifted to 1696 cm^{-1}, the bands at 1634 and 1454 cm^{-1} were widened, the band at 1466 cm^{-1} disappeared, the band at 1326 cm^{-1} was widened and shifted at 1329 cm^{-1}, and the band at 846 cm^{-1} (assigned to the bond C–H aromatic) was shifted to a higher frequency of 849 cm^{-1}. For CP II, the bands at 2957 and 2912 cm^{-1} remain unchanged, while the band at 1122 cm^{-1} (assigned to the bond C–N amide) disappeared, and the bands at 1355 and 692 cm^{-1} were shifted at 1358 and 682 cm^{-1}, respectively. Since FT-IR spectra presented considerable changes of the characteristic ABZ bands, we suggest solid-state interactions between the components of the supramolecular systems obtained by KN and CP methods. In particular, absorption bands attributed to the carbamate group changed; from these events we concluded that the carbamate portion of ABZ interacted with βCD to form an inclusion complex in the solid state.

In contrast, for PM I and PM II spectra, the superposition of the absorption bands of the single components can be observed.

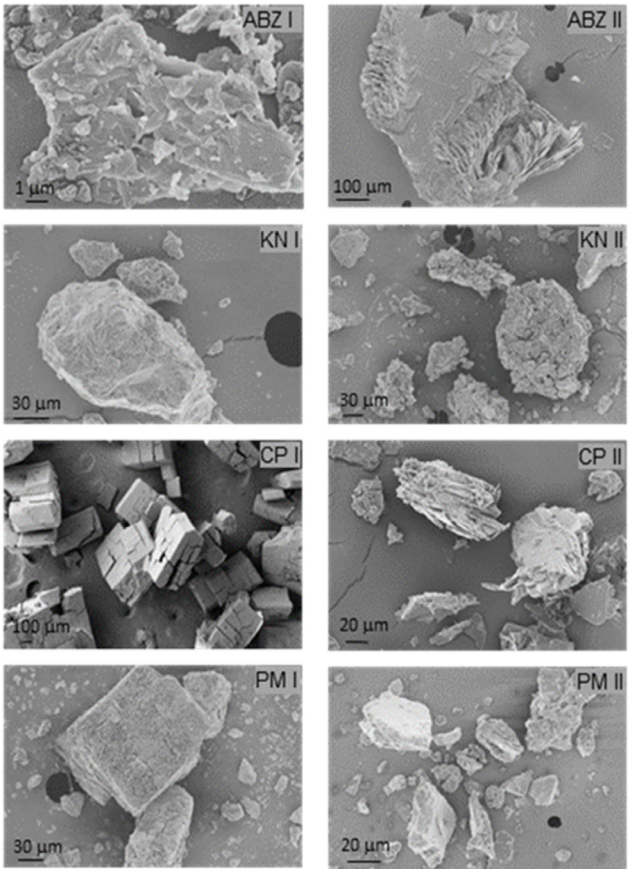

Fig. 5. SEM microphotographs of ABZI, ABZII, and the ABZ I:βCD and ABZ II:βCD systems obtained by kneading (KN) and co-precipitation (CP) methods and physical mixture (PM).

3.2.4. SEM

Scanning electron microscopy was used to examine the microscopic aspects of the materials and it offers supporting evidence for the complexation obtained by different methods of preparation. Fig. 5 illustrates the SEM microphotographs showing the morphological differences between the samples.

ABZ I showed a crystalline structure, with small irregular particles of different sizes and shapes showing a strong tendency to aggregate. ABZ II existed as lamellar particles with a smooth surface that appeared self-agglomerate. While βCD particles had a parallelogram shape with adherences of smaller particles to the surface of large particles (not shown). A drastic change in the morphology of particles was observed in the SEM images of KN and CP systems. The original shape of the raw materials disappeared, and it was not possible to differentiate the single components. The images revealed different types of surface morphologies for KN and CP systems. These changes in the particle shape and aspect suggest the formation of new solid phases, as previously supported by the RMN, PXRD and FT-IR analysis. Both KN systems showed a less ordered structure with irregular compact particles; in particular, KN II was formed by the adherence of particles of different sizes. This is what may contribute to a faster dissolution compared to the CP system. The microphotographs of CP I showed a block structure with numerous cracks and fissures, while CP II existed in a mixture of different size laminate particles with fragile aspect and tendency to agglomerate. On the other hand, the raw materials were clearly detectable in the SEM images of the PMs, thus confirming the presence of the crystalline drug and the absence of interactions.

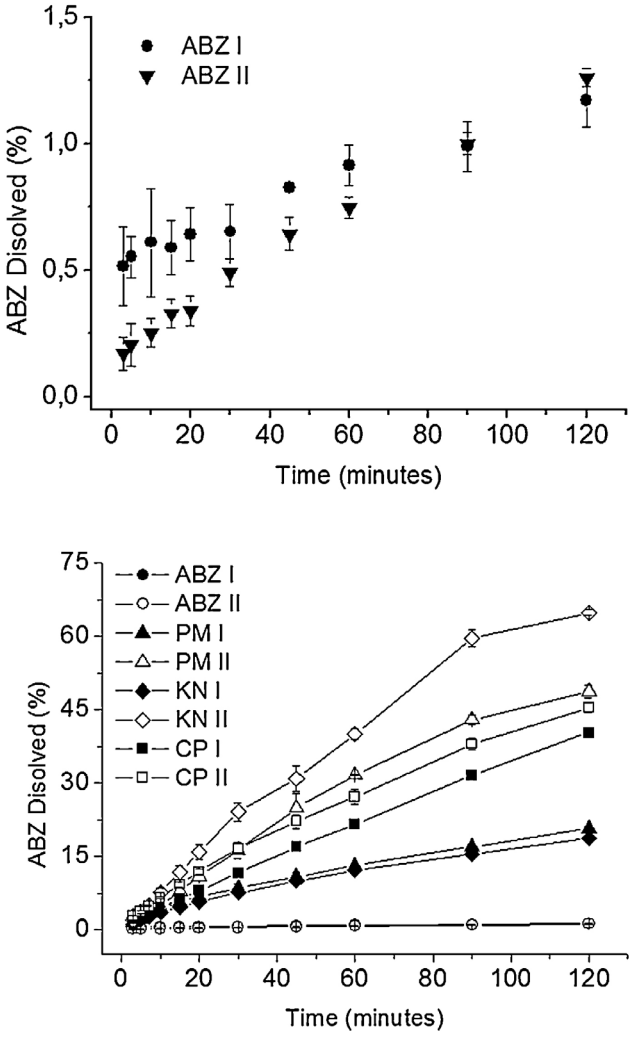

Fig. 6. Dissolution profiles in simulated gastric fluid of ABZI, ABZII, and the ABZ I:βCD and ABZ II:βCD systems obtained by kneading (KN) and co-precipitation (CP) methods and physical mixture (PM).

3.3. Dissolution study

The dissolution experiments were carried out in simulated gastric fluid without enzymes to evaluate the effect of cyclodextrin systems on dissolution rate of the two solid forms of ABZ. The dissolution profiles obtained for ABZ (form I and II) and their corresponding CPs, KNs and PMs systems are presented in Fig. 6.

Comparison of dissolution profiles revealed clear differences in the rate and percentage of dissolution of the different solids under study. As expected, ABZ free base (form I and II) showed the lowest extent of dissolution with 1% of the total drug dissolved after 120 min. Besides, slight differences could be seen between the profiles of the ABZI and ABZII forms (Fig. 6). In addition, significant increases in the percentage of dissolution were evidenced for the profiles and with all binary systems, exhibiting, like this, a dissolution rate faster than the free solid forms. It was determined that KN II produced the highest dissolved percentage for ABZII, showing a 65% of drug dissolved after 120 min. While CP I increased to 40%, the quantity of ABZI dissolved after 120 min.

The significant dissolution enhancement that occurred with KN II, CP II and CP I may be attributed to an increase of solubility upon complexation, and to the decrease of crystalline state that was confirmed by PXRD. On the other hand, the improvement of dissolution

observed with PM may have been due to an in situ solubilization process that produced an increase in the amount of drug dissolved.

Dissolution profiles of the binary systems were compared with those of reference: free ABZI and ABZII, respectively, by applying similarity factor ($f2$). The $f2$ values obtained were 51.9, 36.7, 49.5, 24.0, 32.5 and 31.0 for KN I, CP I, PM I, KN II, CP II and PM II, respectively. Since this $f2$ values were much lower than 100, they are indicating that dissolution profiles of KNs, CPs and PMs systems were not similar to those of the free ABZ forms. These results suggested that the complexes resulting from the interaction with βCD generated a great enhancement of the ABZ dissolution rate.

4. Conclusions

In this study, we have characterized the interactions between the guest ABZI and ABZII and the ligand βCD that resulted in the formation of different binary complexes. The complexation was confirmed by NMR experiments, XRD, FT-IR and SEM in the solid state, as well as by solubility analysis and dissolution studies in solution. The solubility of ABZI and ABZII was improved by the addition of βCD to the complexation medium, both in aqueous solution and in gastric simulated fluid. Furthermore, the increase in ABZ solubility resulting from the formation of supramolecular complexes, significantly favored their dissolution in simulated gastric fluid. In particular, ABZII showed the highest increment of solubility and dissolution rate in simulated gastric fluid. The results obtained for the ABZ II:βCD complexes indicated that they are useful tools for improving the oral bioavailability of ABZ, due to the increase of the drug solubility and dissolution rate in physiological simulated fluids. Due to low and erratic oral bioavailability, ABZ requires the administration of multiple doses to provide therapeutic concentrations. Therefore, these new complexes constitute an interesting alternative for the preparation, on industrial scale, of ABZ pharmaceutical formulations with improve oral bioavailability.

Acknowledgments

This work was supported by FONCyT (Préstamo BID PICT 2013 0504), Consejo Nacional de Investigaciones Científicas y Técnicas (CONICET), Secretaría de Ciencia y Técnica de la Universidad Nacional de Córdoba (SECyT-UNC) and Ministerio de Ciencia y Tecnología (MinCyT) de la Provincia de Córdoba. We want to thank Ferromet S.A. (agent of Roquette in Argentina) for their donation of β-cyclodextrin.

References

Barrera, M. G., Leonardi, D., Bolmaro, R. E., Echenique, C. G., Olivieri, A. C., Salomon, C. J., et al. (2010). In vivo evaluation of albendazole microspheres for the treatment of *Toxocara canis* larva migrans. *European Journal of Pharmaceutics and Biopharmaceutics*, *75*(3), 451–454.

Bauer, J. F. (2008). Pharmaceutical solids: Polymorphism—A critical consideration in pharmaceutical development, manufacturing, and stability. *Journal of Validation Technology*, *14*, 15–23.

Braga, S., Goncalves, I., Herdtweck, E., & Teixeira-Dias, J. (2003). Solid state inclusion com-pound of S-ibuprofen in β-cyclodextrin: Structure and characterisation. *New Journal of Chemistry*, *27*, 597–601.

Brewster, M. E., & Loftsson, T. T. (2007). Cyclodextrins as pharmaceutical solubilizers. *Advanced Drug Delivery Reviews*, *59*, 645–666.

Chattah, A. K., Mroue, K. H., Pfund, L. Y., Ramamoorthy, A., Longhi, M. R., & Garnero, C. (2013). Insights into novel supramolecular complexes of two solid forms of norfloxacin and β-cyclodextrin. *Journal of Pharmaceutical Science*, *102*, 3717–3724.

Chattah, A. K., Zhang, R., Mroue, K. H., Pfund, L. Y., Longhi, M. R., Ramamoorthy, A., et al. (2015). Investigating albendazole desmotropes by solid-state NMR spectroscopy. *Molecular Pharmaceutics*, *12*(3), 731–741.

Codina, A. V., García, A., Leonardi, D., Vasconi, M. D., Di Masso, R. J., Lamas, M. C., et al. (2015). Efficacy of albendazole:β-cyclodextrin citrate in the parenteral stage of *Trichinella spiralis* infection. *International Journal of Biological Macromolecules*, *77*, 203–206.

Cook, G. C. (1990). Use of benzimidazole chemotherapy in human helminthiasis: indications and efficacy. *Parasitology Today*, *6*, 133–136.

Costa, P. (2001). An alternative method to the evaluation of similarity factor in dissolution testing. *International Journal of Pharmaceutics*, *220*, 77–83.

Delrivo, A., Zoppi, A., & Longhi, M. R. (2012). Interaction of sulfadiazine with cyclodextrins in aqueous solution and solid state. *Carbohydrate Polymers*, *87*, 1980–1988.

Dvoroznáková, E., Hrcková, G., Borosková, Z., Velebny, S., & Dubinsky, P. (2004). Effect of treatment with free and liposomized albendazole on selected immunological parameters and cyst growth in mice infected with *Echinococcus multilocularis*. *Parasitology International*, *53*(4), 315–325.

Evrard, B., Chiap, P., DeTullio, P., Ghalmi, F., Piel, G., Van Hees, T., et al. (2002). Oral bioavailability in sheep of albendazole from a suspension and from a solution containing hydroxypropyl-beta-cyclodextrin. *Journal of Controlled Release*, *85*, 45–50.

Ferreira, M. J. G., García, A., Leonardi, D., Salomon, C. J., Lamas, M. C., & Nunes, T. G. (2015). ^{13}C and ^{15}N solid-state NMR studies on albendazole and cyclodextrin albendazole complexes. *Carbohydrate Polymers*, *123*, 130–135.

Gao, Y., Zhao, X., Dong, B., Zheng, L., Li, N., & Zhang, S. (2006). Inclusion complexes of β-cyclodextrin with liquid surfactants. *Journal of Physical Chemistry B*, *110*, 8576–8581.

García, A., Barrera, M. G., Piccirilli, G., Vasconi, M. D., Di Masso, R. J., Leonardi, D., et al. (2013). Novel albendazole formulations given during the intestinal phase of *Trichinella spiralis* infection reduce effectively parasiticmuscle burden inmice. *Parasitology International*, *62*(6), 568–570.

Garnero, C., Chattah, A. K., & Longhi, M. (2013). Supramolecular complexes of Maltodextrin and Furosemide polymophs: A new approach for delivery systems. *Carbohydrate Polymers*, *94*, 292–300.

Garnero, C., Chattah, A. K., & Longhi, M. (2014). Improving furosemide polymorphs properties through supramolecular complexes of β-cyclodextrin. *Journal of Pharmaceutical and Biomededical Analysis*, *95*, 139–145.

Harris, R. K. (1994). *Nuclear magnetic resonance spectroscopy*. London: Logman Scientific and Technical.

Higuchi, T., & Connors, K. A. (1965). *Phase-solubility techniques*. pp. 117–212. *Advances in analytical chemistry and instrumentation* (Vol. 4) New York: Interscience.

Hilfiker, R. (Ed.). (2006). *Polymorphism in the pharmaceutical industry*. Wiley-VCH Verlag GmbH & Co.: KGaA Germany.

Lobenberg, R., & Amidon, G. L. (2000). Modern bioavailability, bioequivalence and biopharmaceutics classification system. New scientific approaches to international regulatory standards. *European Journal of Pharmaceutics and Biopharmaceutics*, *50*, 3–12.

Monti, G. A., Chattah, A. K., & Garro Linck, Y. (2014). Solid-state nuclear magnetic resonance in pharmaceutical compounds. *Annual Reports on NMR Spectroscopy*, *83*, 221–269.

Moore, W. J., & Flanner, H. H. (1996). Mathematical comparison of dissolution profiles. *Pharmaceutical Technology*, *20*, 64–74.

Pensel, P. E., Castro, S., Allemandi, D., Sánchez Bruni, S., Palma, S. D., & Elissondo, M. C. (2014). Enhanced chemoprophylactic and clinical efficacy of albendazole formulated as solid dispersions in experimental cystic echinococcosis. *Veterinary Parasitology*, *203*, 80–86.

Pradines, B., Gallard, J. F., Iorga, B. I., Gueutin, C., Loiseau, P. M., Ponchel, G., & Bouchemal, K. (2014). Investigation of the complexation of albendazole with cyclodextrins for the design of new antiparasitic formulations. *Carbohydrate Research*, *398*, 50–55.

Pranzo, M. B., Cruickshank, D., Coruzzi, M., Caira, M. R., & Bettini, R. (2010). Enantiotropically related albendazole polymorphs. *Journal of Pharmaceutical Science*, *99*(9), 3731–3742.

Zoppi, A., Garnero, C., Garro Linck, Y., Chattah, A. K., Monti, G., & Longhi, M. R. (2011). Enalapril:β-CD complex: Stability. *Carbohydrate Polymers*, *86*, 716–721.